Nano Research 2018, 11(8): 4412–4422
https://doi.org/10.1007/s12274-018-2031-y
Research Article
ISSN 1998-0124
CN 11-5974/O4

Facile synthesis of graphene-supported Ni-CeO_x nanocomposites as highly efficient catalysts for hydrolytic dehydrogenation of ammonia borane

Qilu Yao[1], Zhang-Hui Lu[1] (✉), Yuwen Yang[1], Yuzhen Chen[2], Xiangshu Chen[1] (✉), and Hai-Long Jiang[2] (✉)

[1] *Institute of Advanced Materials (IAM), College of Chemistry and Chemical Engineering, Jiangxi Normal University, Nanchang 330022, China*
[2] *Hefei National Laboratory for Physical Sciences at the Microscale, Collaborative Innovation Center of Suzhou Nano Science and Technology, Department of Chemistry, University of Science and Technology of China, Hefei 230026, China*

Received: 8 December 2017
Revised: 12 February 2018
Accepted: 18 February 2018

KEYWORDS
hydrogen generation,
ammonia borane,
catalysis,
graphene,
nickel

ABSTRACT

Development of low-cost and high-performance catalysts for hydrogen generation via hydrolysis of ammonia borane (NH_3BH_3, AB) is a highly desirable pathway for future hydrogen utilization. In this work, Ni nanocatalysts doped with CeO_x and supported on graphene (Ni-CeO_x/graphene) were synthesized via a facile chemical reduction route and applied as robust catalysts for the hydrolysis of AB in aqueous solution at room temperature. The as-synthesized Ni-CeO_x/graphene nanocomposites (NCs) exhibited excellent catalytic activity with a turnover frequency (TOF) as high as 68.2 min^{-1}, which is 49-fold higher than that for a simple Ni nanoparticle catalyst and is among the highest values reported for non-noble metal catalysts in AB hydrolysis. The development of efficient and low-cost Ni-CeO_x/graphene catalysts enhances the feasibility of using ammonia borane as a chemical hydrogen storage material, which may find application in a hydrogen fuel-cell based economy.

1 Introduction

Hydrogen is regarded as one of the best alternative energy carriers to meet the increasing demand for an effective and clean energy supply due to its abundance, high energy density, and environmental friendliness [1–4]. Effective storage and release of hydrogen are the main technological obstacles in the transformation to a hydrogen-powered society as a possible long-term solution for a secure energy future [5–8]. Recently, ammonia borane (NH_3BH_3, AB) was identified as one of the leading candidates for chemical hydrogen storage because of its high hydrogen content (19.6 wt.%), high stability under ordinary storage conditions, and nontoxicity [9–14]. In addition to the generation of hydrogen via thermal decomposition, hydrolysis of AB in the presence of a suitable catalyst generates three moles of hydrogen gas per mole of AB under mild conditions (Eq. (1)), which makes it an effective approach for hydrogen release from AB [15–20]

Address correspondence to Zhang-Hui Lu, luzh@jxnu.edu.cn; Xiangshu Chen, cxs66cn@jxnu.edu.cn; Hai-Long Jiang, jianglab@ustc.edu.cn

$$NH_3BH_3(aq) + 2H_2O(l) \rightarrow NH_4^+(aq) + BO_2^-(aq) + 3H_2(g) \quad (1)$$

A variety of catalysts have been developed for the hydrolytic dehydrogenation of AB, among which noble metal (Pt, Rh, Ru)-based catalysts are considered state-of-the-art [11, 21–26]. In order to meet the practical application of this system, the development of economical and efficient catalysts to further improve the kinetic properties under moderate conditions remain to be a highly desired goal. Non-noble metal Ni nanocatalysts have been widely used as heterogeneous catalysts for AB hydrolysis, as well as in various industrial chemical reactions, because they have desirable catalytic properties, are more abundant, and are less expensive than noble metal nanocatalysts [27–40]. However, metal nanoparticles (NPs) are naturally prone to aggregation and particle growth because they possess high surface energies. It is well known that the stabilization of small-size metal NPs and suppression of their aggregation during catalysis are crucial factors in their catalytic performance. To remedy this issue, one facile and effective strategy is to anchor the active metal NPs to suitable supports [41]. Graphene, as a single-atom-thick two-dimensional material, exhibits fascinating properties such as high specific surface area, great stability, and outstanding charge carrier mobility, and is therefore an ideal substrate for the growth and anchoring of metal NPs for catalysis [42, 43]. Despite the relatively high cost of graphene, graphene-supported metal NPs have attracted considerable attention owing to their potential applications in many fields such as catalysis, sensors, and energy conversion [42–44]. Recently, metal oxides (such as TiO_2, SnO_2, Fe_3O_4, SiO_2, CeO_2, etc.) have also been widely used as structural and chemical promoters to improve the stability and activity of metal nanocatalysts [45–51]. Among the metal oxides that have been studied, rare-earth oxide CeO_2 is of particular interest owing to its abundant oxygen vacancy defects, high oxygen storage capacity, and cost-effectiveness [46–51]. In this case, given the possible presence of a metal/CeO_2/graphene triple junction, it is proposed that the combination of CeO_2, a metal, and graphene may yield a material with remarkably enhanced activity for the hydrolytic dehydrogenation of AB as well as enhanced stability and dispersibility in the catalytic process.

Herein, we report a green and facile synthesis of well-dispersed Ni-CeO_x/graphene nanocomposites (NCs) in the absence of surfactant. The graphene plays a crucial role in the nucleation and growth of Ni-CeO_x NPs on its surface by providing a large scaffold for anchoring the NPs, owing to its large specific surface area and two-dimensional planar conjugation structure. The CeO_x dopant plays a particularly important role in improving the catalytic performance of the NC through a strong Ni-CeO_x interaction. Unexpectedly, the Ni-CeO_x/graphene NC exhibits remarkable performance in hydrogen generation from AB with a total turnover frequency value as high as 68.2 min^{-1} at room temperature, which is among the highest values reported for non-noble metal catalysts thus far.

2 Experimental

2.1 Chemicals and materials

Ammonia borane (NH_3BH_3, 90%, Aldrich), sodium borohydride ($NaBH_4$, 99%, Aldrich), nickel chloride hexahydrate ($NiCl_2·6H_2O$, ≥ 90%, Sinopharm Chemical Reagent Co. Ltd.), graphene (G250, ≥ 98%, Shanxi Coal Chemical Research Institute of the Chinese Academy of Sciences), cerium (III) nitrate hexahydrate ($Ce(NO_3)_3·6H_2O$, 99.5%, J&K Scientific Ltd.), lanthanum(III) nitrate hexahydrate ($La(NO_3)_3·6H_2O$, 99.9%, J&K Scientific Ltd.), dysprosium(III) nitrate hexahydrate ($Dy(NO_3)_3·6H_2O$, 99.9%, J&K Scientific Ltd.), erbium(III) nitrate pentahydrate ($Er(NO_3)_3·5H_2O$, 99.9%, J&K Scientific Ltd.), terbium(III) nitrate hexahydrate ($Tb(NO_3)_3·6H_2O$, 99.9%, J&K Scientific Ltd.), gadolinium(III) nitrate hexahydrate ($Gd(NO_3)_3·6H_2O$, 99.9%, J&K Scientific Ltd.), and ytterbium(III) nitrate pentahydrate ($Yb(NO_3)_3·5H_2O$, 99.9%, J&K Scientific Ltd.) were used as obtained. Ultrapure water with a specific resistance of 18.3 MΩ·cm was obtained by reverse osmosis, followed by ion exchange and filtration.

2.2 Characterization

Powder X-ray diffraction (XRD) studies were performed on a Rigaku X-ray diffractometer (RINT2000) operated at 40 kV and 40 mA using a Cu Kα radiation source (λ = 1.54178 Å) with a scanning angle (2θ) of 10°–90°. Transmission electron microscopy (TEM), energy-dispersive X-ray (EDS) spectroscopy, and selected-area electron diffraction (SAED) were carried out using an FEI Tecnai

G^2 20 U-Twin TEM instrument operating at 200 kV. Samples for TEM analysis were prepared by depositing a few drops of the catalyst dispersed in ethanol on the amorphous carbon-coated copper grids. X-ray photoelectron spectroscopy (XPS) was carried out on an ESCALAB 250 X-ray photoelectron spectrometer using an Al Kα source. Ar sputtering experiments were performed under a vacuum of 3.2×10^{-6} Pa and at a sputtering acceleration voltage of 1 kV. The atomic ratio of Ni:Ce in the Ni-CeO_x/graphene NC was determined by inductively coupled plasma-atomic emission spectroscopy measurements (ICP-AES; Varian 725-ES).

2.3 Synthesis of catalysts

The Ni-CeO_x/graphene nanocomposites were prepared via a simple and green method at room temperature. Briefly, 10 mg of graphene was dispersed in 5 mL of water by ultrasonication for 30 min at room temperature to obtain a well-dispersed graphene suspension. Then, 21.13 mg of $NiCl_2 \cdot 6H_2O$ (0.08 mmol) and 6.98 mg of $Ce(NO_3)_3 \cdot 6H_2O$ (0.016 mmol) were added to the graphene suspension and stirred for 30 min. Next, a mixture of the reductants $NaBH_4$ (5 mg) and AB (34.3 mg) was added to the above solution with stirring until bubble generation ceased, and the black Ni-CeO_x/graphene NC (17 mol% Ce based on ICP-AES) was obtained.

Other Ni/graphene catalysts with different loadings of Ni (24 wt.%, 28 wt.%, 32 wt.%, 37 wt.%, and 48 wt.% based on ICP-AES) were prepared using the above method by adjusting the amount of graphene (5, 8, 10, 12, and 15 mg, respectively) and omitting the $Ce(NO_3)_3 \cdot 6H_2O$.

Additional Ni-CeO_x/graphene catalysts with different molar compositions (n_{Ce}/n_{Ni+Ce} = 10 mol%, 14 mol%, 20 mol%, and 23 mol%, as determined by ICP-AES) were prepared using the above method and changing the amount of $Ce(NO_3)_3 \cdot 6H_2O$.

For comparison, graphene, CeO_x/graphene, Ni/graphene, and Ni-ReO_x/graphene (Re = La, Tb, Er, Dy, Yb, and Gd, 17 mol% of Re) were also prepared using the method mentioned above.

2.4 Catalytic performance evaluation

The apparatus used for measuring the hydrogen evolution from the hydrolysis of AB was similar to that previously reported [30]. In general, the catalytic reaction was carried out using a 50 mL two-necked round-bottom flask which contained an aqueous suspension of the as-synthesized Ni-CeO_x/graphene NCs (n_{Ni} = 0.08 mmol; 5 mL). One neck of the two-necked round-bottom flask was connected to a gas burette. The reaction flask was placed in a water bath at 298 K under ambient atmosphere. The catalytic reaction began when 34.3 mg of AB (1 mmol) was added to the reaction flask with vigorous magnetic stirring. The evolution of hydrogen was monitored by recording the displacement of water in the gas burette, and the reaction was completed when gas evolution ceased.

The activities of the other catalysts for the hydrolysis of AB were also assessed using the method described above. The molar ratio of n_{Ni}/n_{AB} was kept constant at 0.08 in all the catalytic reactions.

To assess the durability of the catalysts, the catalyzed reactions were repeated 5 times by adding another equivalent of AB (1 mmol) into the reaction flask after completion of the preceding cycle. After the reaction, the Ni-CeO_x/graphene NCs were easily separated from the reaction solution by centrifugation (13,000 rpm, 10 min), washed twice with water and ethanol, and dried under vacuum at 313 K for the TEM analysis.

2.5 Calculation method

The turnover frequency (TOF) values reported herein are total TOF values based on the number of metal atoms in the catalyst, as calculated from Eq. (2)

$$\mathrm{TOF} = n_{H_2}/(n_{Ni} \times t) \quad (2)$$

where n_{H_2} is the moles of H_2 generated, n_{Ni} is the moles of Ni in the catalyst, and t is the total reaction time in minutes.

3 Results and discussion

3.1 Synthesis and characterization of catalysts

The Ni-CeO_x/graphene NCs were synthesized via a green and facile co-reduction method (Scheme 1). First, graphene was dispersed in water by ultrasonication. Subsequently, $NiCl_2 \cdot 6H_2O$ and $Ce(NO_3)_3 \cdot 6H_2O$ were added to the suspension. Finally, $NaBH_4$ and AB were added while the reaction mixture was stirred magnetically at room temperature. In this reaction, $NaBH_4$ and AB act as co-reductants for the reduction of $NiCl_2$ to Ni(0),

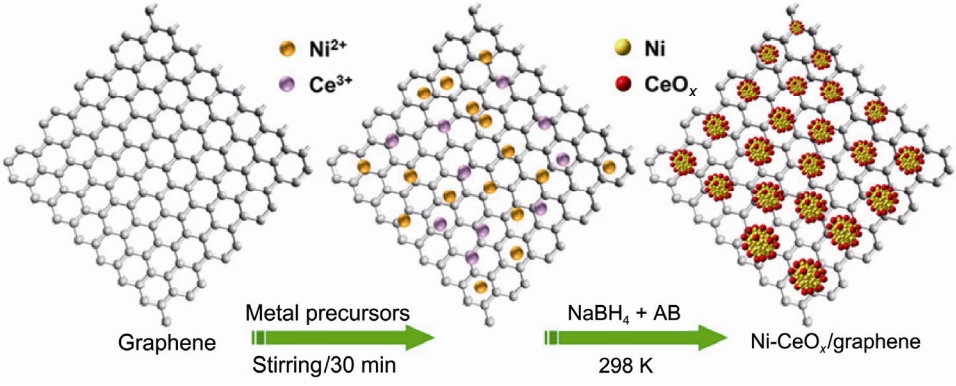

Scheme 1 Schematic illustration of the preparation of Ni-CeO_x/graphenehe morphologies of the synthesized catalysts were characterized by TEM.

while the hydrolysates of $NaBH_4$ and AB provide an alkaline medium (Table S1 in the Electronic Supplementary Material (ESM)) for the formation of CeO_x. It is known that $Ce(NO_3)_3$ is very unstable in alkaline conditions wherein it is easily hydrolyzed to $Ce(OH)_3$ which further reacts with O_2 in the air to form CeO_x (Eqs. (S1) and (S2) in the ESM). CeO_x and Ni NPs may be formed almost simultaneously and serve as the *in situ* seeds for the successive formation of Ni-CeO_x hybrid NPs. Furthermore, the graphene nanosheets play a crucial role in the growth and anchoring of Ni-CeO_x NPs on their surfaces to form the final highly dispersed Ni-CeO_2/graphene NCs.

The morphologies of the obtained catalysts were characterized by transmission electron microscopy (TEM). Figures 1(a)–1(c) display the TEM images of graphene and Ni-CeO_x/graphene NCs, from which wrinkled morphology that graphene intrinsically owns can be observed, and Ni-CeO_x NPs are highly dispersed on the surface of graphene sheets with particle size of around 14 nm (Figs. 1(b) and 1(c)).

The high-resolution TEM (HRTEM) image of Ni-CeO_x/graphene NCs (Fig. S1 in the ESM) does not show lattice fringes, indicating that the material is in an amorphous state. The corresponding EDS spectrum (Fig. S2 in the ESM) validates the presence of Ni, Ce, O, and C. The atomic ratio of Ni:Ce, as determined by ICP-AES was found to be 0.91:0.18, which agreed with the initial value. The element mappings by high-angle annular dark-field scanning transmission electron microscopy (HAADF-STEM) revealed that Ni and Ce are homogeneously distributed in the metal nanoparticles (Fig. 1(c)). In addition, the TEM image of the Ni/graphene NCs (Fig. S3 in the ESM) showed a dispersion pattern similar to that of Ni-CeO_x/graphene (Fig. 1(b)). However, the Ni-CeO_x NPs prepared without graphene were severely aggregated (Fig. S4 in the ESM). These results reveal that graphene nanosheets can effectively stabilize metal NPs.

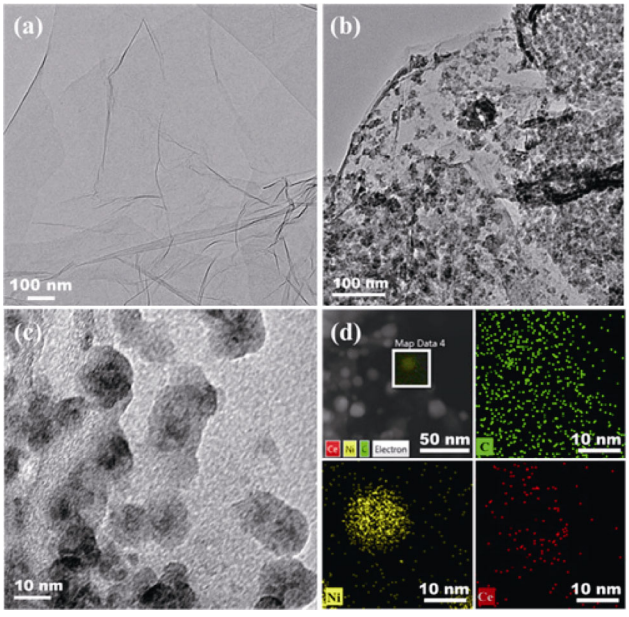

Figure 1 TEM images of (a) graphene and ((b) and (c)) Ni-CeO_x/graphene, (d) HAADF-STEM image of Ni-CeO_x/graphene and the corresponding elemental mapping for C, Ni, and Ce.

XRD patterns of the obtained samples are presented in Fig. 2. For the Ni/graphene catalyst, in addition to the diffraction peak of graphene (2θ = 25.0°), a broad peak was observed at approximately 44.2°, indicating that the Ni NPs had a low degree of crystallinity. No diffraction peaks corresponding to either Ni or CeO_x in the Ni-CeO_x/graphene composite (Fig. 2(d)) and Ni-CeO_x NPs (Fig. 2(c)) were observed, implying that the Ni-CeO_x was in a nearly amorphous state, which was consistent with the HRTEM result (Figs. S1 and S4 in the ESM). After

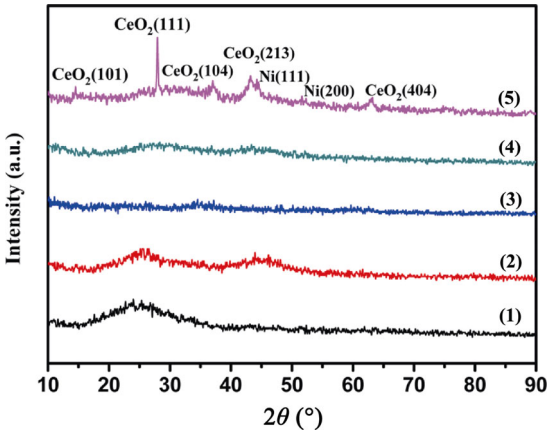

Figure 2 XRD patterns of (1) graphene, (2) Ni/graphene, (3) Ni-CeO_x, (4) Ni-CeO_x/graphene, and (5) Ni-CeO_x/graphene annealed at 773 K for 4 h under N_2 in tube furnace.

annealing at 773 K for 4 h under N_2 in a tube furnace, the XRD peaks of Ni and CeO_x appeared clearly, demonstrating their high crystallinity. Compared with the low-crystallinity catalyst (Ni/graphene), the amorphous catalyst (Ni-CeO_x/graphene) is considered to undergo much more structural distortion and thus has a greater number of active sites for the catalytic reactions [52].

To determine the chemical state of Ni and Ce in Ni-CeO_x/graphene, XPS analysis was performed after Ar sputtering. As shown in Fig. 3(a), the Ni 2p spectrum of the Ni-CeO_x/graphene catalyst mainly shows two peaks at binding energies (BEs) of 852.9 and 870.3 eV, which correspond to the Ni $2p_{3/2}$ and Ni $2p_{1/2}$ photoelectron peaks of the Ni(0) species. In the Ce 3d spectrum of Ni-CeO_x/graphene (Fig. 3(b)), six peaks labeled as U_0, U_1, U_2 ($3d_{5/2}$), U_3, U_4, and U_5 ($3d_{3/2}$) correspond to three pairs of spin–orbit doublets that are characteristic of CeO_2, and another four peaks labeled as V_0, V_1 ($3d_{5/2}$), V_2, and V_3 ($3d_{3/2}$) were ascribed to Ce_2O_3. The atomic ratio of Ce(IV):Ce(III) is determined to be approximately 3:2 by XPS analysis. It has been reported that the valence and defect structures of CeO_x compounds are dynamic and may change spontaneously in response to physical parameters such as the presence of other ions, the partial pressure of oxygen, and temperature [48–51]. Therefore, the existence of both Ce_2O_3 and CeO_2 in Ni-CeO_x/graphene NCs is reasonable. In the O 1s XPS spectrum of Ni-CeO_x/graphene (Fig. S5 in the ESM), the peak near 529.2 eV is assignable to the lattice oxygen in CeO_x, and the peak at 532.0 eV is usually associated with the surface chemisorbed oxygen species

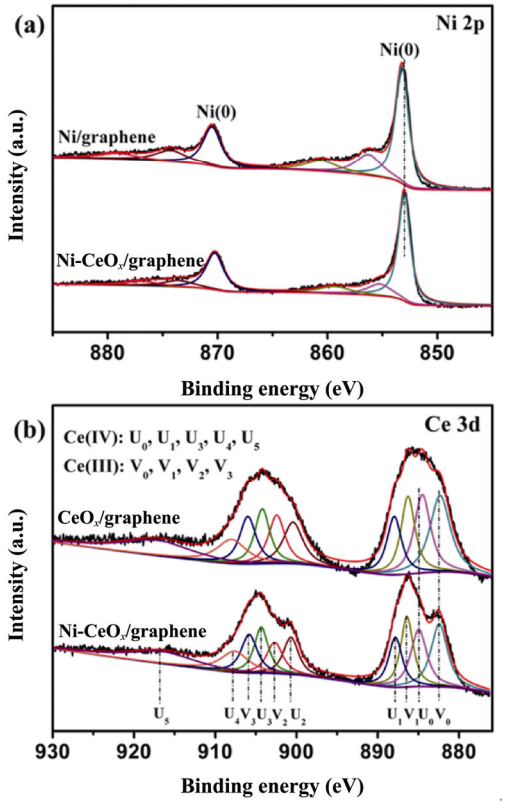

Figure 3 XPS spectra of (a) Ni 2p for the Ni-CeO_x/graphene and Ni/graphene, (b) Ce 3d for the Ni-CeO_x/graphene and CeO_x/graphene.

(H_2O and/or CO_2) [49, 51].

In addition, the XPS spectra showed that the peaks corresponding to Ni (Fig. 3(a)) in Ni-CeO_x/graphene were negatively shifted relative to those of Ni/graphene, whereas the peaks corresponding to Ce (Fig. 3(b)) in the Ni-CeO_x/graphene NCs were positively shifted relative to those of CeO_x/graphene. These shifts indicated that some electrons are transferred from CeO_x to Ni in Ni-CeO_x/graphene, which is confirmed by density functional theory (DFT) calculations where enhanced charge transfer from the defect ceria surface to Ni cluster [53, 54]. Such electron transfer in Ni-CeO_x/graphene is assumed to contribute to improved catalytic activity in the hydrolytic dehydrogenation of AB.

3.2 Catalytic performance

The catalytic activity of the prepared Ni-CeO_x/graphene for hydrogen generation from an aqueous solution of AB was evaluated in a typical water-filled graduated burette system and compared with the catalytic activity

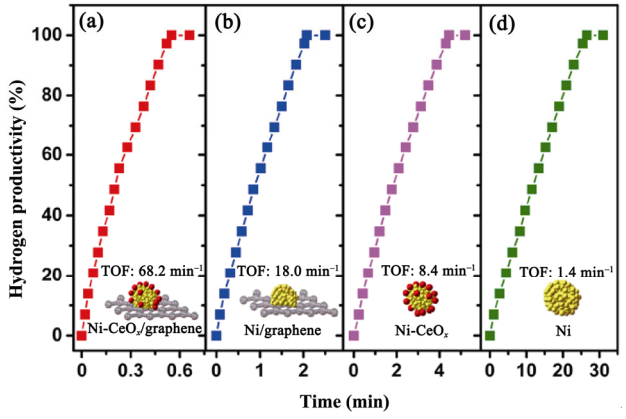

Figure 4 Hydrogen productivity vs. reaction time for hydrogen release from an aqueous AB solution (200 mM, 5 mL) catalyzed by (a) Ni-CeO_x/graphene, (b) Ni/graphene, (c) Ni-CeO_x, and (d) Ni at 298 K (n_{Ni}/n_{AB} = 0.08).

of Ni/graphene, Ni-CeO_x, and Ni NPs. Figure 4 shows the production of hydrogen as a function of reaction time.

The free Ni nanoparticulate catalyst exhibited low activity for this reaction, with a TOF value of 1.4 min^{-1} (Fig. 4(d)). After the Ni nanoparticulate was doped with CeO_x (Ni-CeO_x) or immobilized on graphene nanosheets (Ni/graphene with Ni loading of 32 wt.%, Fig. S6 in the ESM), the catalytic activities were greatly improved as indicated by the TOF values of 8.4 and 18.0 min^{-1}, respectively (Figs. 4(b) and 4(c)). Impressively, the combination of CeO_x and graphene in Ni-CeO_x/graphene NCs showed the highest activity among the as-synthesized catalysts (Fig. 4). The Ni-CeO_x/graphene NC generated a stoichiometric amount of hydrogen (n_{H_2}/n_{AB} = 3) in 0.55 min with a TOF of 68.2 min^{-1} (Fig. 4(a)), which is approximately 49, 8, and 4 times higher than that of Ni NPs (1.4 min^{-1}), Ni-CeO_x NPs (8.4 min^{-1}), and Ni/graphene (18 min^{-1}) under the same conditions, respectively. To the best of our knowledge, this is among the highest reported TOF values for noble-metal-free catalysts used for hydrogen generation via hydrolysis of AB at room temperature (Table 1), and is even comparable to that of a commercial Pt/C catalyst (83.3 min^{-1}) [9, 27–30, 52, 55–64]. It should be noted that neither graphene nor CeO_x/graphene show any catalytic activity (Fig. S7 in the ESM). It is assumed that the catalytic activity of Ni-CeO_x/graphene nanocomposites originates from Ni, while graphene and CeO_x serve as synergists. These results indicate that the rare earth metal oxide CeO_x plays a key role in the synthesis of highly active graphene-based multi-component composite catalysts. The synergistic effect at the interface of the CeO_x, Ni species, and graphene is favorable for catalytic activity, as well as for electron transfer from CeO_x to electron-rich Ni sites, as confirmed

Table 1 Catalytic activity performances of various non-noble metal catalysts for hydrogen generation from the hydrolysis of AB in aqueous solution at room temperature

Catalyst	n_{metal}/n_{AB}	TOF (min^{-1})	E_a ($kJ \cdot mol^{-1}$)	Ref.
$Ni_{0.7}Co_{1.3}P$/GO	0.026	109.4[a]	—	[55]
$Cu_{0.8}Co_{0.2}O$-GO	0.024	70.0	45.5	[56]
Ni-CeO_x/graphene	0.08	68.2	28.9	This work
$Ni_{0.9}Mo_{0.1}$/graphene	0.05	66.7	21.8	[30]
$Ni_{0.7}Co_{1.3}P$	0.026	58.4[a]	43.2	[55]
$Cu_{0.2}Co_{0.8}$/PDA-rGO	0.05	55.6[b]	54.9	[57]
Cu/MIL-101-1-U	0.02	51.4	31.3	[58]
CuCo/MIL-101-1-U	0.02	51.7	30.5	[58]
$Cu_{0.5}Ni_{0.5}$/CMK-1	0.072	54.8	—	[59]
Ni_2P	0.12	40.4	44.6	[29]
In situ Co NPs	0.04	44.1	—	[60]
Ni NPs/ZIF-8	0.03	35.3 (85.7[a])	42.7	[61]
Ni@MSC-30	0.016	30.7	—	[28]
Ni/C	0.0425	8.8	28	[27]
Cu/rGO	0.1	3.6	38.2	[62]
In situ Fe NPs	0.12	3.1	—	[52]
Ni/γ-Al_2O_3	0.018	2.5[c]	—	[63]
Ni^0/CeO_2	0.027	1.7	25	[64]

[a]The reaction was promoted with addition of NaOH. [b]The reaction was carried out at 303 K. [c]The reaction was carried out at 293 K.

by XPS results. Consequently, the activity of Ni-CeO_x/graphene is significantly enhanced.

The catalytic activities of Ni-CeO_x/graphene NCs with various Ce contents (n_{Ce}/n_{Ce+Ni}) were also studied; results are presented in Fig. 5.

It was observed that the catalyst activity depends significantly on the Ce content. As shown in Fig. 5, the catalytic activities of Ni-CeO_x/graphene NCs increased with increasing Ce content up to 17 mol%. However, further increases in the Ce content resulted in an obvious decrease in catalytic activity, which may be due to excess Ce blocking the active Ni sites. The Ni-CeO_x/graphene with 17 mol% of Ce was found to be the most active in the hydrolytic dehydrogenation of AB in the present system.

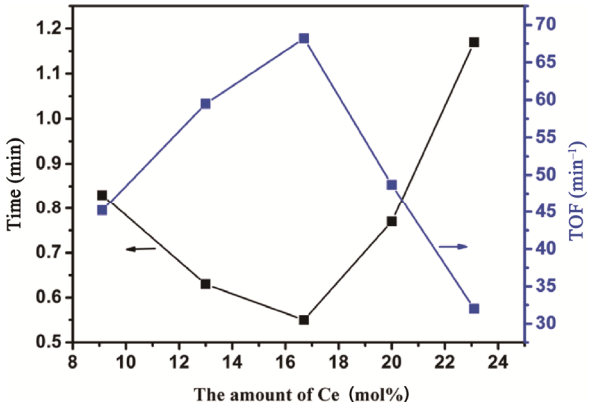

Figure 5 Plots of reaction completion time and the corresponding TOF vs. Ce content (n_{Ce}/n_{Ce+Ni}) in Ni-CeO_x/graphene NCs for hydrogen release from an aqueous AB solution (200 mM, 5 mL) at 298 K (n_{Ni}/n_{AB} = 0.08).

To obtain the activation energy (E_a) of the hydrolysis reaction, the hydrolysis of AB catalyzed by Ni-CeO_x/graphene NCs and Ni/graphene catalysts at different temperatures was also carried out. The results showed that hydrogen generation rates increased when the reaction temperature increased from 298 to 313 K (Fig. 6), suggesting that a high reaction temperature is beneficial for improving the catalytic performance.

The hydrogen generation curves in each plot show slight deviations at the late stage of the hydrolysis reaction (Fig. 6), which is probably due to the external diffusion limit at a very low AB concentration as the catalytic reaction proceeds [21, 65, 66]. In this case, the hydrolysis rate (k) can be determined from the linear portion of each plot. According to the Arrhenius equation, (Eq. (3))

$$\ln(k) = \ln A - E_a/(RT) \quad (3)$$

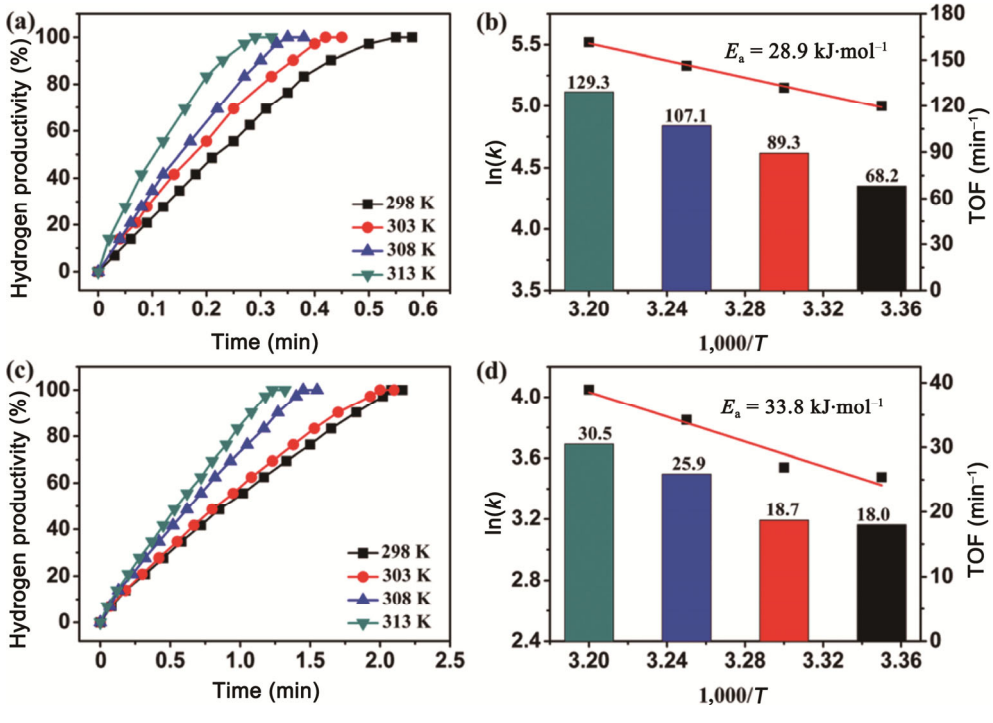

Figure 6 Hydrogen productivity vs. reaction time for hydrogen release from an aqueous AB solution (200 mM, 5 mL) and Arrhenius plots and TOF values of AB hydrolytic dehydrogenation catalyzed by ((a) and (b)) Ni-CeO_x/graphene with 17 mol% of Ce and ((c) and (d)) Ni/graphene at different temperatures in the range of 298–313 K (n_{Ni}/n_{AB} = 0.08).

the E_a for hydrolysis of AB over Ni-CeO_x/graphene is calculated to be 28.9 kJ·mol^{-1} (Fig. 6(b)). This value is lower than that calculated for hydrolysis over Ni/graphene (33.8 kJ·mol^{-1}, Fig. 6(d)) as well as most of the reported activation energy values for the same reaction (Table 1), demonstrating that CeO_x can remarkably improve the reaction kinetics of H_2 generation from the hydrolysis of aqueous AB. A series of control experiments were carried out to explore the kinetics of the catalyzed hydrolytic dehydrogenation of AB. Figure S8(a) in the ESM shows the plots of the volume of hydrogen generated versus time during the catalytic hydrolysis of AB in the presence of different concentrations of Ni. As shown in Fig. S8 in the ESM, the catalytic reactions were completed in 1.17, 0.85, 0.55, and 0.45 min over Ni-CeO_2/graphene with molar ratios (n_{Ni}/n_{AB}) of 0.04, 0.06, 0.08, and 0.1, respectively, corresponding to respective TOF values of 64.1, 58.8, 68.2, and 66.7 min^{-1}. The optimal molar ratio of n_{Ni}/n_{AB} for the catalyzed hydrolysis of AB over Ni-CeO_2/graphene was found to be 0.08. Figure S8(b) in the ESM shows the plot of hydrogen generation rate versus the concentration of Ni on a logarithmic scale. The slope of the trend line was calculated to be 1.09, which was very close to 1 and indicated that the hydrolysis of AB catalyzed by Ni-CeO_x/graphene is first order with respect to the Ni concentration.

The stability of the Ni-CeO_x/graphene and Ni/graphene catalysts in terms of reusability was also tested at 298 K under ambient atmosphere, as shown in Fig. S9 in the ESM. Over five runs, there was no significant decrease in catalytic activity of the Ni-CeO_x/graphene catalyst, while an obvious decrease was noted in the catalytic activity of the Ni/graphene catalyst. As seen in the TEM image (Fig. S10 in the ESM), there was no noticeable change in the morphology of Ni-CeO_x/graphene after the durability test. These results reveal that the combination of CeO_x, Ni, and graphene can elicit materials with remarkably enhanced catalytic activity as well as stability.

Since cerium oxide effectively improved the catalytic activity of Ni/graphene, some other rare-earth metal oxides (ReO_x, Re = La, Dy, Er, Yb, Gd, and Tb) were used as dopants in Ni/graphene composites (Ni-ReO_x/graphene). These were prepared by the same method described for the synthesis of Ni-CeO_x/graphene, and their catalytic activities for the hydrolysis of AB were studied and compared (Fig. 7).

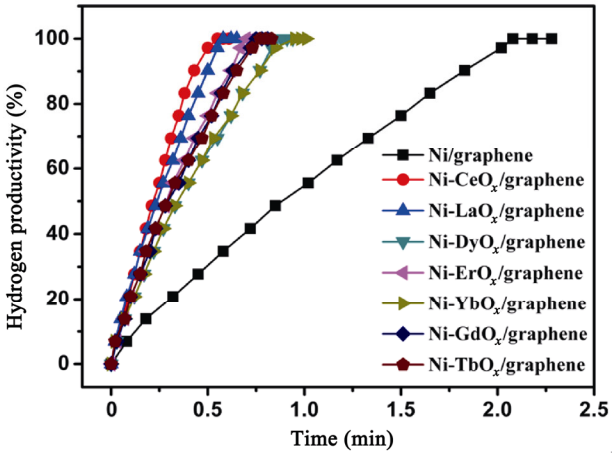

Figure 7 Hydrogen productivity vs. reaction time for hydrogen release from an aqueous AB solution (200 mM, 5 mL) catalyzed by Ni/graphene and Ni-ReO_x/graphene (Re = Ce, La, Dy, Er, Yb, Gd, and Tb, 17 mol% of Re) at 298 K (n_{Ni}/n_{AB} = 0.08).

As shown in Fig. 7, all the as-synthesized Ni-ReO_x/graphene composites exhibited higher catalytic activities than Ni/graphene, producing a stoichiometric amount of hydrogen (n_{H_2}/n_{AB} = 3) in 1 min. The excellent activities of the Ni-ReO_x/graphene composites may be attributed to the similar physical and chemical properties of ReO_x species which all promote active sites of Ni to electron-rich states that are beneficial to the catalytic reaction [67]. Interestingly, among the as-synthesized Ni-ReO_x/graphene composites, Ni-CeO_x/graphene exhibited the best performance. However, Ni-LaO_x/graphene also demonstrated a high catalytic activity with a TOF of 64.7 min^{-1} at room temperature.

4 Conclusions

In summary, we have developed a novel, facile and green strategy for the synthesis of Ni-CeO_x/graphene nanocomposites. The rare-earth metal oxide species CeO_x played a key role in the high activity of graphene-based multi-component composite catalysts. The combination of CeO_x, metal, and graphene confers remarkably enhanced catalytic activity for the hydrolytic dehydrogenation of ammonia borane, as well as high stability. This improvement in the catalytic performance of the Ni-CeO_x/graphene composite encourages the practical application of AB as a hydrogen storage material in fuel cell applications. Furthermore, it is expected that the synthesis of Ni-CeO_x/graphene ternary hybrid materials

will pave the way for the design of other graphene-based multicomponent composites for various applications. It is believed that this kind of nanocatalyst will have great potential in future industrial applications.

Acknowledgements

This work was financially supported by the National Natural Science Foundation of China (Nos. 21763012, 21463012, 21371162, 21673213, and 21521001), the Natural Science Foundation of Jiangxi Province of China (Nos. 20171ACB21021 and 2016BAB203087), and the National Research Fund for Fundamental Key Project (No. 2014CB931803).

Electronic Supplementary Material: Supplementary material (related TEM images, EDX spectrum, XPS spectra, results of catalytic hydrolytic dehydrogenation of AB, and durability results of catalysts) is available in the online version of this article at https://doi.org/10.1007/s12274-018-2031-y.

References

[1] Chen, P.; Xiong, Z. T.; Luo, J. Z.; Lin, J. Y.; Tan, K. L. Interaction of hydrogen with metal nitrides and imides. *Nature* **2002**, *420*, 302–304.

[2] Yan, H.; Lin, Y.; Wu, H.; Zhang, W. H.; Sun, Z. H.; Cheng, H.; Liu, W.; Wang, C. L.; Li, J. J.; Huang, X. H. et al. Bottom-up precise synthesis of stable platinum dimers on graphene. *Nat. Commun.* **2017**, *8*, 1070.

[3] Wang, N.; Sun, Q. M.; Bai, R. S.; Li, X.; Guo, G. Q.; Yu, J. H. *In situ* confinement of ultrasmall Pd clusters within nanosized silicalite−1 zeolite for highly efficient catalysis of hydrogen generation. *J. Am. Chem. Soc.* **2016**, *138*, 7484–7487.

[4] Zhang, J. J.; Kang, Q.; Yang, Z. Q.; Dai, H. B.; Zhuang, D. W.; Wang, P. A cost-effective NiMoB-La(OH)$_3$ catalyst for hydrogen generation from decomposition of alkaline hydrous hydrazine solution. *J. Mater. Chem. A* **2013**, *1*, 11623–11628.

[5] Peng, B.; Chen, J. Ammonia borane as an efficient and lightweight hydrogen storage medium. *Energy Environ. Sci.* **2008**, *1*, 479–483.

[6] Wang, J.; Li, W.; Wen, Y. R.; Gu, L.; Zhang, Y. Rh-Ni-B nanoparticles as highly efficient catalysts for hydrogen generation from hydrous hydrazine. *Adv. Energy Mater.* **2015**, *5*, 1401879.

[7] Tang, C.; Zhang, R.; Lu, W. B.; He, L. B.; Jiang, X. E.; Asiri, A. M.; Sun, X. P. Fe-doped CoP nanoarray: A monolithic multifunctional catalyst for highly efficient hydrogen generation. *Adv. Mater.* **2017**, *29*, 1602441.

[8] Bi, Q. Y.; Lin, J. D.; Liu, Y. M.; He, H. Y.; Huang F. Q.; Cao, Y. Dehydrogenation of formic acid at room temperature: Boosting palladium nanoparticle efficiency by coupling with pyridinic-nitrogen-doped carbon. *Angew. Chem., Int. Ed.* **2016**, *55*, 11849–11853.

[9] Chandra, M.; Xu, Q. A high-performance hydrogen generation system: Transition metal-catalyzed dissociation and hydrolysis of ammonia-borane. *J. Power Sources* **2006**, *156*, 190–194.

[10] Demirci, U. B.; Miele, P. Sodium borohydride versus ammonia borane, in hydrogen storage and direct fuel cell applications. *Energy Environ. Sci.* **2009**, *2*, 627–637.

[11] Zhan, W.; Zhu, Q. L.; Xu, Q. Dehydrogenation of ammonia borane by metal nanoparticle catalysts. *ACS Catal.* **2016**, *6*, 6892–6905.

[12] Kang, J. X.; Chen, T. W.; Zhang, D. F.; Guo, L. PtNiAu trimetallic nanoalloys enabled by a digestive-assisted process as highly efficient catalyst for hydrogen generation. *Nano Energy* **2016**, *23*, 145–152.

[13] Zhang, H.; Gu, X. J.; Liu, P. L.; Song, J.; Cheng, J.; Su, H. Q. Highly efficient visible-light-driven catalytic hydrogen evolution from ammonia borane using non-precious metal nanoparticles supported by graphitic carbon nitride. *J. Mater. Chem. A* **2017**, *5*, 2288–2296.

[14] Lu, Z. H.; Li, J. P.; Zhu, A. L.; Yao, Q. L.; Huang, W.; Zhou, R. Y.; Zhou, R. F.; Chen, X. S. Catalytic hydrolysis of ammonia borane via magnetically recyclable copper iron nanoparticles for chemical hydrogen storage. *Int. J. Hydrogen Energy* **2013**, *38*, 5330–5337.

[15] Gutowska, A.; Li, L. Y.; Shin, Y.; Wang, C. M.; Li, X. S.; Linehan, J. C.; Smith, R. S.; Kay, B. D.; Schmid, B.; Shaw, W. et al. Nanoscaffold mediates hydrogen release and the reactivity of ammonia borane. *Angew. Chem., Int. Ed.* **2005**, *44*, 3578–3582.

[16] Jiang, H. L.; Xu, Q. Catalytic hydrolysis of ammonia borane for chemical hydrogen storage. *Catal. Today* **2011**, *170*, 56–63.

[17] Chen, W. Y.; Li, D. L.; Wang, Z. J.; Qian, G.; Sui, Z. J.; Duan, X. Z.; Zhou, X. G.; Yeboah, I.; Chen, D. Reaction mechanism and kinetics for hydrolytic dehydrogenation of ammonia borane on a Pt/CNT catalyst. *AIChE J.* **2017**, *63*, 60–65.

[18] Ge, Y. Z.; Ye, W. Y.; Shah, Z. H.; Lin, X. J.; Lu, R. W.; Zhang, S. F. PtNi/NiO clusters coated by hollow sillica: Novel design for highly efficient hydrogen production from ammonia-borane. *ACS Appl. Mater. Interfaces* **2017**, *9*, 3749–3756.

[19] Zhou, L. M.; Meng, J.; Li, P.; Tao, Z. L.; Mai, L. Q.; Chen, J. Ultrasmall cobalt nanoparticles supported on nitrogen-doped porous carbon nanowires for hydrogen evolution from ammonia borane. *Mater. Horiz.* **2017**, *4*, 268–273.

[20] Yao, Q. L.; Lu, Z. H.; Zhang, Z. J.; Chen, X. S.; Lan, Y. Q. One-pot synthesis of core-shell Cu@SiO$_2$ nanospheres and their

catalysis for hydrolytic dehydrogenation of ammonia borane and hydrazine borane. *Sci. Rep.* **2014**, *4*, 7597.

[21] Chen, W. Y.; Ji, J.; Feng, X.; Duan, X. Z.; Qian, G.; Li, P.; Zhou, X. G.; Chen, D.; Yuan, W. K. Mechanistic insight into size-dependent activity and durability in Pt/CNT catalyzed hydrolytic dehydrogenation of ammonia borane. *J. Am. Chem. Soc.* **2014**, *136*, 16736–16739.

[22] Khalily, M. A.; Eren, H.; Akbayrak, S.; Susapto, H. H.; Biyikli, N.; Özkar, S.; Guler, M. O. Facile synthesis of three-dimensional Pt-TiO_2 nano-networks: A highly active catalyst for the hydrolytic dehydrogenation of ammonia-borane. *Angew. Chem., Int. Ed.* **2016**, *55*, 12257–12261.

[23] Akbayrak, S.; Tonbul, Y.; Özkar, S. Ceria supported rhodium nanoparticles: Superb catalytic activity in hydrogen generation from the hydrolysis of ammonia borane. *Appl. Catal. B: Environ.* **2016**, *198*, 162–170.

[24] Akbayrak, S.; Özkar, S. Ruthenium(0) nanoparticles supported on multiwalled carbon nanotube as highly active catalyst for hydrogen generation from ammonia-borane. *ACS Appl. Mater. Interfaces* **2012**, *4*, 6302–6310.

[25] Yao, Q. L.; Shi, W. M.; Feng, G.; Lu, Z. H.; Zhang, X. L.; Tao, D. J.; Kong, D. J.; Chen, X. S. Ultrafine Ru nanoparticles embedded in SiO_2 nanospheres: Highly efficient catalysts for hydrolytic dehydrogenation of ammonia borane. *J. Power Sources* **2014**, *257*, 293–299.

[26] Yao, Q. L.; Lu, Z. H.; Jia, Y. S.; Chen, X. S.; Liu, X. *In situ* facile synthesis of Rh nanoparticles supported on carbon nanotubes as highly active catalysts for H_2 generation from NH_3BH_3 hydrolysis. *Int. J. Hydrogen Energy* **2015**, *40*, 2207–2215.

[27] Metin, O.; Mazumder, V.; Özkar, S.; Sun, S. S. Monodisperse nickel nanoparticles and their catalysis in hydrolytic dehydrogenation of ammonia borane. *J. Am. Chem. Soc.* **2010**, *132*, 1468–1469.

[28] Li, P. Z.; Aijaz, A.; Xu, Q. Highly dispersed surfactant-free nickel nanoparticles and their remarkable catalytic activity in the hydrolysis of ammonia borane for hydrogen generation. *Angew. Chem., Int. Ed.* **2012**, *51*, 6753–6756.

[29] Peng, C. Y.; Kang, L.; Cao, S.; Chen, Y.; Lin, Z. S.; Fu, W. F. Nanostructured Ni_2P as a robust catalyst for the hydrolytic dehydrogenation of ammonia–borane. *Angew. Chem., Int. Ed.* **2015**, *54*, 15725–15729.

[30] Yao, Q. L.; Lu, Z. H.; Huang, W.; Chen, X. S.; Zhu, J. Highly Pt-like activity of Ni-Mo/graphene catalyst for hydrogen evolution from hydrolysis of ammonia borane. *J. Mater. Chem. A* **2016**, *4*, 8579–8583.

[31] Chen, G. Z.; Desinan, S.; Rosei, R.; Rosei, F.; Ma, D. L. Synthesis of Ni-Ru alloy nanoparticles and their high catalytic activity in dehydrogenation of ammonia borane. *Chem. Eur. J.* **2012**, *18*, 7925–7930.

[32] Li, P. Z.; Aranishi, K.; Xu, Q. ZIF-8 immobilized nickel nanoparticles: Highly effective catalysts for hydrogen generation from hydrolysis of ammonia borane. *Chem. Commun.* **2012**, *48*, 3173–3175.

[33] Cao, C. Y.; Chen, C. Q.; Li, W.; Song, W. G.; Cai, W. Nanoporous nickel spheres as highly active catalyst for hydrogen generation from ammonia borane. *ChemSusChem* **2010**, *3*, 1241–1244.

[34] Lu, Z. H.; Li, J. P.; Feng, G.; Yao, Q. L.; Zhang, F.; Zhou, R. Y.; Tao, D. J.; Chen, X. S.; Yu, Z. Q. Synergistic catalysis of MCM-41 immobilized Cu-Ni nanoparticles in hydrolytic dehydrogeneration of ammonia borane. *Int. J. Hydrogen Energy* **2014**, *39*, 13389–13395.

[35] Du, X. Q.; Yang, C. L.; Zeng, X.; Wu, T.; Zhou, Y. H.; Cai, P.; Cheng, G. Z.; Luo, W. Amorphous NiP supported on rGO for superior hydrogen generation from hydrolysis of ammonia borane. *Int. J. Hydrogen Energy* **2017**, *42*, 14181–14187.

[36] Zhang, J. K.; Chen, C. Q.; Yan, W. J.; Duan, F. F.; Zhang, B.; Gao, Z.; Qin, Y. Ni Nanoparticles supported on CNTs with excellent activity produced by atomic layer deposition for hydrogen generation from the hydrolysis of ammonia borane. *Catal. Sci .Technol.* **2016**, *6*, 2112–2119.

[37] De, S.; Zhang, J. G.; Luque; R.; Yan, N. Ni-based bimetallic heterogeneous catalysts for energy and environmental applications. *Energy Environ. Sci*. **2016**, *9*, 3314–3347.

[38] Zhou, L. M.; Zhang, T. R.; Tao, Z. L.; Chen, J. Ni nanoparticles supported on carbon as efficient catalysts for the hydrolysis of ammonia borane. *Nano Res.* **2014**, *7*, 774–781.

[39] Du, J.; Cheng, F. Y.; Si, M.; Liang, J. Tao, Z. L.; Chen, J. Nanoporous Ni-based catalysts for hydrogen generation from hydrolysis of ammonia borane. *Int. J. Hydrogen Energy* **2013**, *38*, 5768–5774.

[40] Yang, X. J.; Cheng, F. Y.; Liang, J.; Tao, Z. L.; Chen, J. Carbon-supported $Ni_{1-x}@Pt_x$ (x = 0.32, 0.43, 0.60, 0.67, and 0.80) core–shell nanoparticles as catalysts for hydrogen generation from hydrolysis of ammonia borane. *Int. J. Hydrogen Energy* **2011**, *36*, 1984–1990.

[41] Zhu, Q. L.; Xu, Q. Immobilization of ultrafine metal nanoparticles to high-surface-area materials and their catalytic applications. *Chem*. **2016**, *1*, 220–245.

[42] Wang, J.; Zhang, X. B.; Wang, Z. L.; Wang, L. M.; Zhang, Y. Rhodium-nickel nanoparticles grown on graphene as highly efficient catalyst for complete decomposition of hydrous hydrazine at room temperature for chemical hydrogen storage. *Energy Environ. Sci.* **2012**, *5*, 6885–6888.

[43] Yang, L.; Luo, W.; Cheng, G. Z. Graphene-supported Ag-based core-shell nanoparticles for hydrogen generation in hydrolysis of ammonia borane and methylamine borane. *ACS Appl. Mater. Interfaces* **2013**, *5*, 8231–8240.

[44] Wang, Y.; Arandiyan, H.; Scott, J.; Bagheri, A.; Dai, H. X.; Amal, R. Recent advances in ordered meso/macroporous metal

oxides for heterogeneous catalysis: A review. *J. Mater. Chem. A* **2017**, *5*, 8825–8846.

[45] Singh, V.; Joung, D.; Zhai, L.; Das, S.; Khondaker, S. I.; Sea, S. Graphene based materials: Past, present and future. *Prog. Mater. Sci.* **2011**, *56*, 1178–1271.

[46] Wang, X.; Liu, D. P.; Song, S. Y.; Zhang, H. J. Pt@CeO_2 multicore@shell self-assembled nanospheres: Clean synthesis, structure optimization, and catalytic applications, *J. Am. Chem. Soc.* **2013**, *135*, 15864–15872.

[47] Song, S. Y.; Li, K.; Pan, J.; Wang, F.; Li, J. Q.; Feng, J.; Yao, S.; Ge, X.; Wang, X.; Zhang, H. J. Achieving the trade-off between selectivity and activity in semihydrogenation of alkynes by fabrication of (asymmetrical Pd@Ag core)@(CeO_2 shell) nanocatalysts *via* autoredox reaction. *Adv. Mater.* **2017**, *29*, 1605332.

[48] Zhu, F. F.; Chen, G. Z.; Sun, S. X.; Sun, X. *In situ* growth of Au@CeO_2 core–shell nanoparticles and CeO_2 nanotubes from $Ce(OH)CO_3$ nanorods. *J. Mater. Chem. A* **2013**, *1*, 288–294.

[49] Du, X. Q.; Liu, C.; Du, C.; Cai, P.; Cheng, G. Z.; Luo, W. Nitrogen-doped graphene hydrogel-supported NiPt-CeO_x nanocomposites and their superior catalysis for hydrogen generation from hydrazine at room temperature. *Nano Res.* **2017**, *10*, 2856–2865.

[50] Zhang, Z. J.; Lu, Z. H.; Tan, H. L.; Chen, X. S.; Yao, Q. L. CeO_x-modified RhNi nanoparticles grown on rGO as highly efficient catalysts for complete hydrogen generation from hydrazine borane and hydrazine. *J. Mater. Chem. A* **2015**, *3*, 23520–23529.

[51] Yao, Q. L.; Shi, Y.; Zhang, X. L.; Chen, X. S.; Lu, Z. H. Facile synthesis of platinum–cerium(IV) oxide hybrids arched on reduced graphene oxide catalyst in reverse micelles with high activity and durability for hydrolysis of ammonia borane. *Chem. Asian J.* **2016**, *11*, 3251–3257.

[52] Yan, J. M.; Zhang, X. B.; Han, S.; Shioyama, H.; Xu, Q. Iron-nanoparticle-catalyzed hydrolytic dehydrogenation of ammonia borane for chemical hydrogen storage. *Angew. Chem., Int. Ed.* **2008**, *47*, 2287–2289.

[53] Shishkin, M.; Ziegler, T. The electronic structure and chemical properties of a Ni/CeO_2 anode in a solid oxide fuel cell: A DFT + U study. *J. Phys. Chem. C* **2010**, *114*, 21411–21416.

[54] Hahn, K. R.; Seitsonen, A. P.; Iannuzzi, M.; Hutter, J. Functionalization of CeO_2(111) by deposition of small Ni clusters: Effects on CO_2 adsorption and O vacancy formation. *ChemCatChem* **2015**, *7*, 625–634.

[55] Hou, C. C.; Li, Q.; Wang, C. J.; Peng, C. Y.; Chen, Q. Q.; Ye, H. F.; Fu, W. F.; Che, C. M.; López, N.; Chen, Y. Ternary Ni–Co–P nanoparticles as noble-metal-free catalysts to boost the hydrolytic dehydrogenation of ammonia-borane. *Energy Environ. Sci.* **2017**, *10*, 1770–1776.

[56] Feng, K.; Zhong, J.; Zhao, B. H.; Zhang, H.; Xu, L.; Sun, X. H.; Lee, S. T. $Cu_xCo_{1-x}O$ nanoparticles on graphene oxide as a synergistic catalyst for high-efficiency hydrolysis of ammonia–borane. *Angew. Chem., Int. Ed.* **2016**, *55*, 11950–11954.

[57] Song, F. Z.; Zhu, Q. L.; Yang, X. C.; Xu, Q. Monodispersed CuCo nanoparticles supported on diamine-functionalized graphene as a non-noble metal catalyst for hydrolytic dehydrogenation of ammonia borane. *ChemNanoMat* **2016**, *2*, 942–945.

[58] Liu, P. L.; Gu, X. J.; Kang, K.; Zhang, H.; Cheng; J.; Su, H. Q. Highly efficient catalytic hydrogen evolution from ammonia borane using the synergistic effect of crystallinity and size of noble-metal-free nanoparticles supported by porous metal-organic frameworks. *ACS Appl. Mater. Interfaces* **2017**, *9*, 10759–10767.

[59] Yen, H.; Seo, Y.; Kaliaguine, S.; Kleitz, F. Role of metal-support interactions, particle size, and metal-metal synergy in CuNi nanocatalysts for H_2 generation. *ACS Catal.* **2015**, *5*, 5505–5511.

[60] Yan, J. M.; Zhang, X. B.; Shioyama, H.; Xu, Q. Room temperature hydrolytic dehydrogenation of ammonia borane catalyzed by Co nanoparticles. *J. Power Sources* **2010**, *195*, 1091–1094.

[61] Wang, C. L.; Tuninetti, J.; Wang, Z.; Zhang, C.; Ciganda, R.; Salmon, L.; Moya, S.; Ruiz, J.; Astruc, D. Hydrolysis of ammonia-borane over Ni/ZIF−8 nanocatalyst: High efficiency, mechanism, and controlled hydrogen release. *J. Am. Chem. Soc.* **2017**, *139*, 11610–11615.

[62] Yang, Y. W.; Lu, Z. H.; Hu, Y. J.; Zhang, Z. J.; Shi, W. M.; Chen, X. S.; Wang, T. T. Facile *in situ* synthesis of copper nanoparticles supported on reduced graphene oxide for hydrolytic dehydrogenation of ammonia borane. *RSC Adv.* **2014**, *4*, 13749–13752.

[63] Xu, Q.; Chandra, M. Catalytic activities of non-noble metals for hydrogen generation from aqueous ammonia-borane at room temperature. *J. Power Sources* **2006**, *163*, 364–370.

[64] Akbayrak, S.; Taneroğlu, O.; Özkar, S. Nanoceria supported cobalt(0) nanoparticles: A magnetically separable and reusable catalyst in hydrogen generation from the hydrolysis of ammonia borane. *New J. Chem.* **2017**, *41*, 6546–6552.

[65] Liao, J. Y.; Li, H.; Zhang, X. B.; Feng, K. J.; Yao, Y. L. Fabrication of a Ti-supported $NiCo_2O_4$ nanosheet array and its superior catalytic performance in the hydrolysis of ammonia borane for hydrogen generation. *Catal. Sci. Technol.* **2016**, *6*, 3893–3899.

[66] Yao, Q. L.; Yang, K.; Hong, X. L.; Chen, X. S.; Lu, Z. H. Base-promoted hydrolytic dehydrogenation of ammonia borane catalyzed by noble-metal-free nanoparticles. *Catal. Sci. Technol.* **2018**, *8*, 870–877.

Li, Z.; He, T.; Liu, L.; Chen, W. D.; Zhang, M.; Wu, G. T.; Chen, P. Covalent triazine framework supported non-noble metal nanoparticles with superior activity for catalytic hydrolysis of ammonia borane: From mechanistic study to catalyst design. *Chem. Sci.* **2017**, *8*, 781–788.